Waveguide self-coupling based reconfigurable resonance structure for optical filtering and delay

Linjie Zhou,* Tong Ye, and Jianping Chen

State Key Laboratory of Advanced Optical Communication Systems and Networks
Department of Electronic Engineering, Shanghai Jiao Tong University, Shanghai 200240, China
**ljzhou@sjtu.edu.cn*

Abstract: We propose a novel waveguide self-coupling based reconfigurable resonance structure to work as a flat-top second-order tunable filter and a tunable delay line with low group delay dispersion. The high-order resonance features result from the mutual mode coupling between the clockwise and counter-clockwise resonance eigenmodes. The transfer-matrix method is used to theoretically analyze the device optical performances. The relations between the two embedded phase shifters for achieving flat-top filtering and group delay responses are given. As the coupled resonances are provided by only one physical resonator, the device is inherently more compact and resilient to fabrication errors compared to conventional microring resonators. Phase tuning for its reconfiguration is also simpler and more power-efficient.

OCIS codes: (230.3120) Integrated optics devices; (230.5750) Resonators; (130.7408) Wavelength filtering devices.

References and links

1. Y. Vlasov, W. Green, and F. Xia, "High-throughput silicon nanophotonic wavelength-insensitive switch for on-chip optical networks," Nat. Photonics **2**(4), 242–246 (2008).
2. B. Lee, A. Biberman, N. Sherwood-Droz, C. Poitras, M. Lipson, and K. Bergman, "High-speed 2 × 2 switch for multiwavelength siliconphotonic networks-on-chip," J. Lightwave Technol. **27**(14), 2900–2907 (2009).
3. K. Preston, S. Manipatruni, A. Gondarenko, C. B. Poitras, and M. Lipson, "Deposited silicon high-speed integrated electro-optic modulator," Opt. Express **17**(7), 5118–5124 (2009).
4. G. Reed, G. Mashanovich, F. Gardes, and D. Thomson, "Silicon optical modulators," Nat. Photonics **4**(8), 518–526 (2010).
5. Q. Xu, B. Schmidt, S. Pradhan, and M. Lipson, "Micrometre-scale silicon electro-optic modulator," Nature **435**(7040), 325–327 (2005).
6. B. Little, S. Chu, H. Haus, J. Foresi, and J. Laine, "Microring resonator channel dropping filters," J. Lightwave Technol. **15**(6), 998–1005 (1997).
7. L. Zhou, and A. W. Poon, "Fano resonance-based electrically reconfigurable add-drop filters in silicon microring resonator-coupled Mach-Zehnder interferometers," Opt. Lett. **32**(7), 781–783 (2007).
8. L. Zhou, and A. W. Poon, "Electrically reconfigurable silicon microring resonator-based filter with waveguide-coupled feedback," Opt. Express **15**(15), 9194–9204 (2007).
9. J. E. Cunningham, I. Shubin, X. Zheng, T. Pinguet, A. Mekis, Y. Luo, H. Thacker, G. Li, J. Yao, K. Raj, and A. V. Krishnamoorthy, "Highly-efficient thermally-tuned resonant optical filters," Opt. Express **18**(18), 19055–19063 (2010).
10. M. S. Dahlem, C. W. Holzwarth, A. Khilo, F. X. Kärtner, H. I. Smith, and E. P. Ippen, "Reconfigurable multi-channel second-order silicon microring-resonator filterbanks for on-chip WDM systems," Opt. Express **19**(1), 306–316 (2011).
11. P. Dong, N. N. Feng, D. Feng, W. Qian, H. Liang, D. C. Lee, B. J. Luff, T. Banwell, A. Agarwal, P. Toliver, R. Menendez, T. K. Woodward, and M. Asghari, "GHz-bandwidth optical filters based on high-order silicon ring resonators," Opt. Express **18**(23), 23784–23789 (2010).
12. Q. Li, M. Soltani, S. Yegnanarayanan, and A. Adibi, "Design and demonstration of compact, wide bandwidth coupled-resonator filters on a siliconon- insulator platform," Opt. Express **17**(4), 2247–2254 (2009).

#140999 - $15.00 USD Received 13 Jan 2011; revised 1 Apr 2011; accepted 1 Apr 2011; published 12 Apr 2011

13. A. Canciamilla, M. Torregiani, C. Ferrari, F. Morichetti, R. De La Rue, A. Samarelli, M. Sorel, and A. Melloni, "Silicon coupled-ring resonator structures for slow light applications: potential, impairments and ultimate limits," J. Opt. **12**(10), 104008 (2010).
14. J. Heebner, and R. Boyd, "'Slow' and 'fast' light in resonator-coupled waveguides," J. Mod. Opt. **49**(14), 2629–2636 (2002).
15. Q. Li, Z. Zhang, J. Wang, M. Qiu, and Y. Su, "Fast light in silicon ring resonator with resonance-splitting," Opt. Express **17**(2), 933–940 (2009).
16. X. Luo, H. Chen, and A. W. Poon, "Electro-optical tunable time delay and advance in silicon microring resonators," Opt. Lett. **35**(17), 2940–2942 (2010).
17. A. Melloni, F. Morichetti, C. Ferrari, and M. Martinelli, "Continuously tunable 1 byte delay in coupled-resonator optical waveguides," Opt. Lett. **33**(20), 2389–2391 (2008).
18. F. Xia, L. Sekaric, and Y. Vlasov, "Ultracompact optical buffers on a silicon chip," Nat. Photonics **1**(1), 65–71 (2007).
19. J. Cardenas, M. A. Foster, N. Sherwood-Droz, C. B. Poitras, H. L. Lira, B. Zhang, A. L. Gaeta, J. B. Khurgin, P. Morton, and M. Lipson, "Wide-bandwidth continuously tunable optical delay line using silicon microring resonators," Opt. Express **18**(25), 26525–26534 (2010).
20. X. Zheng, I. Shubin, G. Li, T. Pinguet, A. Mekis, J. Yao, H. Thacker, Y. Luo, J. Costa, K. Raj, J. E. Cunningham, and A. V. Krishnamoorthy, "A tunable 1x4 silicon CMOS photonic wavelength multiplexer/demultiplexer for dense optical interconnects," Opt. Express **18**(5), 5151–5160 (2010).
21. A. Agarwal, P. Toliver, R. Menendez, S. Etemad, J. Jackel, J. Young, T. Banwell, B. E. Little, S. T. Chu, and W. Chen, "Fully programmable ring-resonator-based integrated photonic circuit for phase coherent applications," J. Lightwave Technol. **24**(1), 77–87 (2006).
22. J. B. Khurgin, "Expanding the bandwidth of slow-light photonic devices based on coupled resonators," Opt. Lett. **30**(5), 513–515 (2005).
23. J. B. Khurgin, and P. A. Morton, "Tunable wideband optical delay line based on balanced coupled resonator structures," Opt. Lett. **34**(17), 2655–2657 (2009).
24. L. Tobing, S. Darmawan, D. Lim, M. Chin, and T. Mei, "Relaxation of Critical Coupling Condition and Characterization of Coupling-Induced Frequency Shift in Two-Ring Structures," IEEE J. Sel. Top. Quantum Electron. **16**(1), 77–84 (2010).
25. M. Popovic, C. Manolatou, and M. Watts, "Coupling-induced resonance frequency shifts in coupled dielectric multi-cavity filters," Opt. Express **14**(3), 1208–1222 (2006).
26. B. E. Little, J. P. Laine, and S. T. Chu, "Surface-roughness-induced contradirectional coupling in ring and disk resonators," Opt. Lett. **22**(1), 4–6 (1997).
27. B. E. Little, S. T. Chu, and H. A. Haus, "Second-order filtering and sensing with partially coupled traveling waves in a single resonator," Opt. Lett. **23**(20), 1570–1572 (1998).
28. F. Morichetti, A. Canciamilla, M. Martinelli, A. Samarelli, R. De La Rue, M. Sorel, and A. Melloni, "Coherent backscattering in optical microring resonators," Appl. Phys. Lett. **96**(8), 081112 (2010).
29. L. Liao, D. Samara-Rubio, M. Morse, A. Liu, D. Hodge, D. Rubin, U. Keil, and T. Franck, "High speed silicon Mach-Zehnder modulator," Opt. Express **13**(8), 3129–3135 (2005).
30. C. Madsen, and J. Zhao, *Optical Filter Design and Analysis: A Signal Processing Approach* (Wiley, New York, 1999).
31. R. Soref, and B. Bennett, "Electrooptical effects in silicon," IEEE J. Quantum Electron. **23**(1), 123–129 (1987).
32. G. Lenz, B. Eggleton, C. Madsen, and R. Slusher, "Optical delay lines based on optical filters," IEEE J. Quantum Electron. **37**(4), 525–532 (2001).
33. L. B. Soldano, and E. C. M. Pennings, "Optical multi-mode interference devices based on self-imaging: principles and applications," J. Lightwave Technol. **13**(4), 615–627 (1995).
34. L. Zhou, K. Okamoto, and S. Yoo, "Athermalizing and trimming of slotted silicon microring resonators with UV-sensitive PMMA upper-cladding," IEEE Photon. Technol. Lett. **21**(17), 1175–1177 (2009).

1. Introduction

Silicon optical microring resonator is one of the basic building blocks for future integrated photonic circuits due to its compact size and versatile functionalities. It has attracted considerable research interests in recent years, and various kinds of functional devices have been implemented based on microring resonators including switches [1, 2], modulators [3–5], filters [6–12], optical delay lines [13–19], WDM multiplexers [20], and phase coherent devices [21]. For a single microring resonator, its Lorentzian resonance line-shape cannot satisfy the ideal "box-like" spectrum requirement for an optical filter [6]. Its large group delay dispersion (GDD) around resonance also causes distortion to the transmitted optical signal [14]. Hence, coupled resonators in series- or parallel-coupling configurations are always used to improve the filtering and delay performances [10–12, 19, 22, 23].

#140999 - $15.00 USD Received 13 Jan 2011; revised 1 Apr 2011; accepted 1 Apr 2011; published 12 Apr 2011

Due to fabrication errors, however, it is hard to accurately align the resonance frequencies for all resonators and their coupling coefficients can also easily deviate from designed values. These uncertainties will eventually deteriorate the device performances. In addition, coupling can also induce resonance frequency shifts (CIFS) [24, 25], which can further complicate the device design in compensation for this effect. Therefore, there is a great need for fewer resonators to accomplish the same function. One way to reduce the number of resonators is to couple different resonance modes in one physical resonator to get the desired high-order resonance features. A single microring resonator with clockwise (CW) and counter-clockwise (CCW) degenerate resonance modes is quite suitable for this purpose, as its resonances are "auto-aligned" with each other and any fluctuation in the resonator physical parameters can affect these modes equivalently. The coupling between CW and CCW modes can be enabled by small perturbations inside the resonator, which can be a notch or just fabrication-induced sidewall roughness [15, 26–28]. The perturbations cause backscattering, which leads to the resonance splitting and broadening. However, these perturbations are usually very small in the nanometer scale and almost impossible to be fabricated in a controlled way, resulting in reliability issues. Moreover, the coupling strength, which determines the resonance splitting level, is fixed and difficult to be changed once the device is fabricated, further limiting its application.

Based on the counter-propagation mode coupling, in this paper we propose a novel reconfigurable optical resonance structure to perform as a second-order resonance system. Compared to the microring resonator with backward coupling, it overcomes the shortcoming of relying on perturbation to induce mutual mode coupling. Instead, the mode coupling is enabled by waveguide evanescent coupling and thus can be easily controlled and made tunable. As the CW and CCW modes are possessed by one physical resonator, changing one resonator means simultaneously changing two modes, and thus tuning is more power-efficient. Our device features compact size, easy reconfiguration, and high tolerance to fabrication errors, suitable for optical filtering and delay applications.

2. Device structure

Figure 1 shows the schematic structure of our proposed device, which is essentially a single waveguide folded to self-couple with itself to form resonances. Light from the input port passes the first coupler (input coupler) and splits into two paths. At the second coupler (crossing coupler), part of the light crosses over and propagates forward and part is reflected back. The two branches of forward propagating light recombine at the third coupler (output coupler) and the recombined light either circulates back to the input coupler or directly couples out. Therefore, the forward propagating light passes three couplers to form a CW resonance loop, indicated by the large blue arrows in Fig. 1. Similarly, the reflected light travels backward to form a CCW resonance loop, indicated by the small red arrows in Fig. 1. The crossing coupler determines the mutual mode coupling strength between the CW and CCW resonance modes. Light can be reflected back via the CW and CCW resonance loops to the input end. As both the CW and CCW resonance modes are excited, a standing-wave pattern is formed in the resonator.

In order to conveniently control the mutual mode coupling strength, we use a push-pull Mach-Zehnder Interferometer (MZI) [29] to replace the crossing coupler, as shown by the inset in Fig. 1. We also add another push-pull phase shifter in the split paths so that the resonance input/output coupling can be varied (to be proved by theoretical analyses). With these two phase shifters incorporated, the device transmission and reflection spectra can be easily tailored, as will be seen in the following sections.

#140999 - $15.00 USD Received 13 Jan 2011; revised 1 Apr 2011; accepted 1 Apr 2011; published 12 Apr 2011

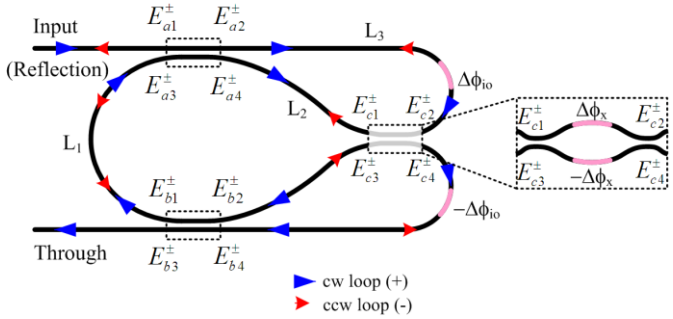

Fig. 1. Schematic of the waveguide self-coupling based reconfigurable resonance structure. Electric fields before and after each coupler are labeled. The Large blue and small red arrows indicate the clockwise (CW) and counter-clockwise (CCW) resonance loops, respectively.

3. Modeling

We use the transfer matrix method to get the transmission and reflection transfer functions of the device [30]. The electric fields before and after each coupler are labeled in Fig. 1, with superscript ' + ' indicating left to right propagation and '-' for right to left propagation.

The electric fields before and after input/output couplers are related by the following transfer matrix:

$$\begin{bmatrix} E_{a2}^{+} \\ E_{a4}^{+} \\ E_{b2}^{+} \\ E_{b4}^{+} \end{bmatrix} = M_{cio} \begin{bmatrix} E_{a1}^{+} \\ E_{a3}^{+} \\ E_{b1}^{+} \\ E_{b3}^{+} \end{bmatrix} = \begin{bmatrix} t_a & -i\kappa_a & 0 & 0 \\ -i\kappa_a & t_a & 0 & 0 \\ 0 & 0 & t_b & -i\kappa_b \\ 0 & 0 & -i\kappa_b & t_b \end{bmatrix} \begin{bmatrix} E_{a1}^{+} \\ E_{a3}^{+} \\ E_{b1}^{+} \\ E_{b3}^{+} \end{bmatrix}, \quad (1)$$

where t_i and κ_i ($i = a, b$ for input and output directional couplers) are the transmission and coupling coefficients of the couplers. Assuming lossless coupling, we have $t_i^2+\kappa_i^2 = 1$. The electric fields then pass four waveguide sections before reaching the MZI crossing coupler, and thus we have

$$\begin{bmatrix} E_{c2}^{-} \\ E_{c1}^{+} \\ E_{c3}^{+} \\ E_{c4}^{-} \end{bmatrix} = M_{t1} \begin{bmatrix} E_{a2}^{+} \\ E_{a4}^{+} \\ E_{b2}^{+} \\ E_{b4}^{+} \end{bmatrix} = \begin{bmatrix} e^{-i(n_{eff}k_0L_3+\Delta\phi_{io})} & 0 & 0 & 0 \\ 0 & e^{-in_{eff}k_0L_2} & 0 & 0 \\ 0 & 0 & e^{-in_{eff}k_0L_2} & 0 \\ 0 & 0 & 0 & e^{-i(n_{eff}k_0L_3-\Delta\phi_{io})} \end{bmatrix} \begin{bmatrix} E_{a2}^{+} \\ E_{a4}^{+} \\ E_{b2}^{+} \\ E_{b4}^{+} \end{bmatrix}, \quad (2)$$

where $\pm\Delta\phi_{io}$ are the phase shifts in the split paths, $n_{eff} = n_{eff}^{'} - in_{eff}^{''}$ is the waveguide complex effective refractive index with $n_{eff}^{'}$ associated with light propagation and $n_{eff}^{''}$ with waveguide propagation loss, $k_0 = 2\pi/\lambda$ is the light propagation constant in free space, and λ is the free space wavelength. The transfer matrix for the MZI crossing coupler (consisting of a pair of 3-dB couplers and a push-pull phase shifter) is

$$\begin{bmatrix} E_{c2}^{+} \\ E_{c1}^{-} \\ E_{c3}^{-} \\ E_{c4}^{+} \end{bmatrix} = M_{cx} \begin{bmatrix} E_{c2}^{-} \\ E_{c1}^{+} \\ E_{c3}^{+} \\ E_{c4}^{-} \end{bmatrix} = \begin{bmatrix} 0 & -i\sin(\Delta\phi_x) & -i\cos(\Delta\phi_x) & 0 \\ -i\sin(\Delta\phi_x) & 0 & 0 & -i\cos(\Delta\phi_x) \\ -i\cos(\Delta\phi_x) & 0 & 0 & i\sin(\Delta\phi_x) \\ 0 & -i\cos(\Delta\phi_x) & i\sin(\Delta\phi_x) & 0 \end{bmatrix} \begin{bmatrix} E_{c2}^{-} \\ E_{c1}^{+} \\ E_{c3}^{+} \\ E_{c4}^{-} \end{bmatrix}, \quad (3)$$

#140999 - $15.00 USD Received 13 Jan 2011; revised 1 Apr 2011; accepted 1 Apr 2011; published 12 Apr 2011

where $\pm\Delta\phi_x$ are the phase shifts in the MZI arms. We can use the same transfer matrices M_{t1}, M_{cio} to describe the field transfer from right to left. At the resonator left side, the electric fields $E_{a3}^{\pm}$ and $E_{b1}^{\pm}$ are related by the bending waveguide L_1, and thus we have

$$\begin{bmatrix} E_{a1}^{+} \\ E_{a3}^{+} \\ E_{b1}^{+} \\ E_{b3}^{+} \end{bmatrix} = M_{t2} \begin{bmatrix} E_{a1}^{+} \\ E_{a3}^{-} \\ E_{b1}^{-} \\ E_{b3}^{+} \end{bmatrix} = \begin{bmatrix} 1 & 0 & 0 & 0 \\ 0 & 0 & e^{-in_{eff}k_0L_1} & 0 \\ 0 & e^{-in_{eff}k_0L_1} & 0 & 0 \\ 0 & 0 & 0 & 1 \end{bmatrix} \begin{bmatrix} E_{a1}^{+} \\ E_{a3}^{-} \\ E_{b1}^{-} \\ E_{b3}^{+} \end{bmatrix}. \tag{4}$$

Combining Eqs. (1)-(4), we get

$$\begin{bmatrix} E_{a1}^{-} \\ E_{a3}^{-} \\ E_{b1}^{-} \\ E_{b3}^{-} \end{bmatrix} = M \begin{bmatrix} E_{a1}^{+} \\ E_{a3}^{-} \\ E_{b1}^{-} \\ E_{b3}^{+} \end{bmatrix} = M_{cio}M_{t1}M_{cx}M_{t1}M_{cio}M_{t2} \begin{bmatrix} E_{a1}^{+} \\ E_{a3}^{-} \\ E_{b1}^{-} \\ E_{b3}^{+} \end{bmatrix}. \tag{5}$$

Assuming the input is only from the upper waveguide, *i.e.*, $E_{a1}^{+} = E_{in}$ and $E_{b3}^{+} = 0$, then E_{a1}^{-} is the reflected electric field and E_{b3}^{-} is the transmitted electric field. Solving the linear equation Eq. (5), we can get the electric field transfer functions for the transmission and reflection ports. To simplify our analysis, we only consider the case when the input and output couplers are ideal 3-dB couplers, *i.e.*, $t_a^2 = t_b^2 = 0.5$, and the transmission and reflection functions are expressed as (in z-domain):

$$H_t(z) = \frac{E_{b3}^{-}}{E_{in}} = t_{wg}t_x \frac{t_{io} - t_x(t_{io}^2+1)az^{-1} + t_{io}a^2z^{-2}}{1 - 2t_xt_{io}az^{-1} + (\kappa_x^2 + t_x^2t_{io}^2)a^2z^{-2}}, \tag{6}$$

$$H_r(z) = \frac{E_{a1}^{-}}{E_{in}} = e^{-i\Delta\phi_{io}}t_{wg}\kappa_x \frac{1 - 2t_xt_{io}az^{-1} + a^2z^{-2}}{1 - 2t_xt_{io}az^{-1} + (\kappa_x^2 + t_x^2t_{io}^2)a^2z^{-2}}, \tag{7}$$

where $z^{-1} = e^{-i\phi} = e^{-i\left(n_{eff}^{'}k_0L+\pi\right)}$ is the CW/CCW round-trip unit delay in the resonator, ϕ is the round-trip phase change, $L = L_1+L_2+L_3$ is the round-trip physical length, $a = e^{-n_{eff}^{''}k_0L}$ is the loss factor representing one CW/CCW round-trip field transmission, $t_{io} = \cos(\Delta\phi_{io})$ and $\kappa_{io} = \sin(\Delta\phi_{io})$ are the resonator input/output effective transmission and coupling coefficients, $t_x = \cos(\Delta\phi_x)$ and $\kappa_x = \sin(\Delta\phi_x)$ are the resonator effective mutual-mode transmission and coupling coefficients, $t_{wg} = -e^{-in_{eff}k_0(L_2+L_3)}$ is the electric field transmission directly from the input-port to the through-port. The phase shifts $\Delta\phi_{io}$ and $\Delta\phi_x$ determine the resonator input/output and crossing coupling strengths, respectively. In silicon, phase shifts can be obtained by using the free carrier plasma dispersion effect [31].

4. Analysis and discussion

The transmission and reflection responses of our structure are dependent on the two phase shifts $\Delta\phi_{io}$ and $\Delta\phi_x$. The resonance structure can be reconfigured for different applications by tuning these two parameters. In the following subsections, we first consider several limiting cases and then analyze its optical performances as a tunable filter and a delay line. The device tolerance to structural parameters and temperature variations is discussed in the last subsection.

#140999 - $15.00 USD Received 13 Jan 2011; revised 1 Apr 2011; accepted 1 Apr 2011; published 12 Apr 2011

4.1 limiting cases

In certain special configurations, the resonance structure can regress to simpler structures, which can be regarded as the limiting cases for our device.

When $\Delta\phi_{io} = 0$ (or $t_{io} = 1$), the amplitude responses for the transmission and reflection ports are $|H_t(z)| = |t_x|$ and $|H_r(z)| = |\kappa_x|$, which implies light is partially reflected (without forming resonances) and its reflectivity is determined by the cross coupling coefficient. When $\Delta\phi_x$ varied from 0 to $\pi/2$, the reflection increases from zero to full reflection.

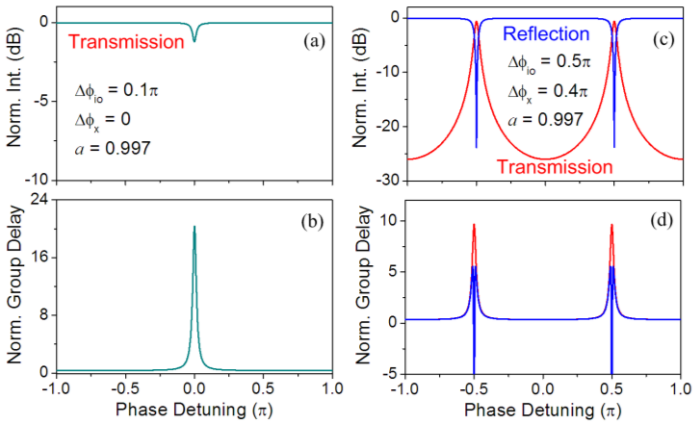

Fig. 2. (a) and (b) Transmission intensity and group delay responses for the device configured as a notch filter. (c) and (d) Transmission and reflection intensity and group delay responses for the device configured as an add-drop filter.

When $\Delta\phi_x = 0$ (or $t_x = 1$), the crossing coupling is at its maximum and the light just crosses over without inducing backward coupling. The transmission function can then be simplified to

$$H_t(z) = t_{wg}\frac{t_{io} - az^{-1}}{1 - t_{io}az^{-1}}, \tag{8}$$

which is essentially the transfer function for a microring notch filter cascaded with a waveguide. Resonances occur at $\phi = 2m\pi$ (m is an integer) and the effective resonator round-trip length is L. The waveguide-resonator coupling coefficient is κ_{io}, which can be controlled by tuning $\Delta\phi_x$. A typical transmission spectrum is shown in Fig. 2(a). As the phase changes rapidly around resonance, a large group delay can be obtained at the resonance frequency. Group delay is the first order derivative of the phase with respect to angular frequency. Group delay can be positive or negative, corresponding to slow light (pulse delay) or fast light (pulse advance) phenomenon. Letting Φ be the phase of the transmission function, then the group delay is $\tau_g = -d\Phi/d\omega = -(d\Phi/d\phi)T_R$, where $T_R = (n_{eff} + \omega dn_{eff}/d\omega)L/c = n_gL/c$ is the light round-trip transmission time, n_g is the waveguide group refractive index, and ω is the angular frequency. Figure 2(b) shows the normalized group delay (τ_g/T_R) for the transmission port. As only a single resonance is formed in the resonator, the intensity and group delay spectra both exhibit sharp peaks.

When $\Delta\phi_{io} = \pi/2$ (or $t_{io} = 0$), the device transfer functions then become

$$H_t(z) = t_{wg}\frac{-t_x^2 az^{-1}}{1 + \kappa_x^2 a^2 z^{-2}}, \tag{9}$$

$$H_r(z) = e^{-i\Delta\phi_{io}} t_{wg}\frac{\kappa_x + \kappa_x a^2 z^{-2}}{1 + \kappa_x^2 a^2 z^{-2}}, \tag{10}$$

#140999 - $15.00 USD Received 13 Jan 2011; revised 1 Apr 2011; accepted 1 Apr 2011; published 12 Apr 2011

which are essentially the transfer functions for an add-drop filter (ADF) cascaded with a waveguide (reflection port has an extra phase shift $\Delta\phi_{io}$). Resonances occur at $\phi = m\pi$-$\pi/2$. Its free spectral range (FSR) is a half smaller than that in the previous case. It means that in this configuration the resonator effective circumference is $2L$. Figures 2(c) and 2(d) show the intensity and group delay spectra for a typical set of parameters.

When $\Delta\phi_x = \pi/2$ (or $t_x = 0$), all the light is reflected back at the crossing coupler and the device is essentially composed by two separate Sagnac loop mirrors. If the input and output couplers are ideal 3-dB couplers, then all the light can be reflected back to the input-port.

4.2 Tunable filter

When both $\Delta\phi_x$ and $\Delta\phi_{io}$ are small, the mutual mode coupling between the CW and CCW resonance modes and the coupling to the external access waveguide are both weak, and then we can configure the device as a second-order filter. The complex poles of the transfer equations Eqs. (6) and (7) are essentially the complex eigenmodes of the device. The complex phase of the pole can be written as $\tilde{\phi}_{p0} = \pm\phi_{p0} + i\gamma/2$, where ϕ_{p0} and γ are associated with the real-valued resonance frequency and linewidth:

$$\phi_{p0} = \tan^{-1}\left(\frac{\kappa_x}{t_x t_{io}}\right), \tag{11}$$

$$\gamma = -\ln\left(t_x^2 t_{io}^2 + \kappa_x^2\right) - 2\ln a. \tag{12}$$

The resonance structure has two eigenmodes with split frequencies and identical linewidths. When their frequency separation is less than the linewidth, *i.e.*, $2\phi_{p0} < \gamma$, these two modes are regarded as undistinguishable. Under weak coupling ($t_{io} \approx 1$ and $t_x \approx 1$), the condition for the undistinguishable eigenmodes can be approximated to

$$\kappa_{io} > \sqrt{2\left(\kappa_x / t_x + \ln a\right)}\,/\,t_x. \tag{13}$$

In order to make use of mode mutual-coupling to expand the passband for a filter application, Eq. (13) should be satisfied.

To get a flat-top passband, the coupling coefficients k_{io} and k_x should satisfy a more stringent requirement. Stating from the pole and zero positions and their function on reflection spectrum, we deduce the relation between the poles and zeros required to generate a flat-top passband. The reflection transfer function has two conjugate poles (p_0 and p_0*) and two conjugate zeros (z_0 and z_0*):

$$p_0 = |p_0| e^{i\phi_{p0}} = a(t_x t_{io} + i\kappa_x), \tag{14}$$

$$z_0 = |z_0| e^{i\phi_{z0}} = a[t_x t_{io} + i\sqrt{1-(t_x t_{io})^2}]. \tag{15}$$

The conjugate poles correspond to two split peaks. When the poles are closer to each other or farther away from the unit circle, the linewidth of the peaks becomes larger than their separation and these two peaks will merge into one and we can no longer distinguish them (see Eq. (13)). Hence, the spectral profile between the poles shown as a peak or a valley is quite dependent on the pole positions in the unit circle.

The existence of the conjugate zeros further tailors the spectrum. The poles and zeros have an identical real part $at_x t_{io}$, but the zeros have a larger imaginary part than the poles have, meaning that the zeros are located outside the poles in the pole-zero diagram, *i.e.*, $\phi_{z0} > \phi_{p0}$. Thus, the addition of zeros makes the reflection passband smoother and also drop faster. To get an exact flat passband, the second-order derivative of the intensity transfer function should be zero at the uncoupled resonance frequency, *i.e.*, $d^2[|H_r(z)|^2]/d\phi^2 = 0$ at $\phi = 0$. After mathematical treatment, we get the following condition for the flat-top passband response:

#140999 - $15.00 USD Received 13 Jan 2011; revised 1 Apr 2011; accepted 1 Apr 2011; published 12 Apr 2011

$$\frac{\left(z_0^* + z_0\right)}{\left|1 - z_0\right|^2} - \frac{\left|z_0 - z_0^*\right|^2}{\left|1 - z_0\right|^4} = \frac{\left(p_0^* + p_0\right)}{\left|1 - p_0\right|^2} - \frac{\left|p_0 - p_0^*\right|^2}{\left|1 - p_0\right|^4}. \tag{16}$$

Equation (16) states the relationship between the poles and zeros, which can be converted to an expression for tuning parameters $\Delta\phi_{io}$ and $\Delta\phi_x$.

Figure 3(a) shows the relation curves between $\Delta\phi_{io}$ and $\Delta\phi_x$ for various loss factors to satisfy the flat-top passband response. The addition of the waveguide propagation loss up-shifts the $\Delta\phi_x$ versus $\Delta\phi_{io}$ curve, which means strong mutual mode coupling is needed to compensate for the loss-induced resonance broadening. The solid curves in Fig. 3(b) show the reflection spectra of our device for three different $\Delta\phi_{io}$'s under the flat-top condition. The intensity remains almost flat between the pole frequencies. Beyond the pole frequencies, the intensity drops rapidly and reaches the minimum around the zero frequencies. Beyond the zeros, the intensity increases slightly. To compare with a conventional microring ADF, we also plot the drop spectra of a double-ring ADF (dotted curves) with its waveguide-ring and ring-ring coupling coefficients being κ_{io} and κ_x, respectively. From the comparison, we see that our device has a faster roll-off but a lower out-of-band rejection ratio because of the excess zeros in the transfer function.

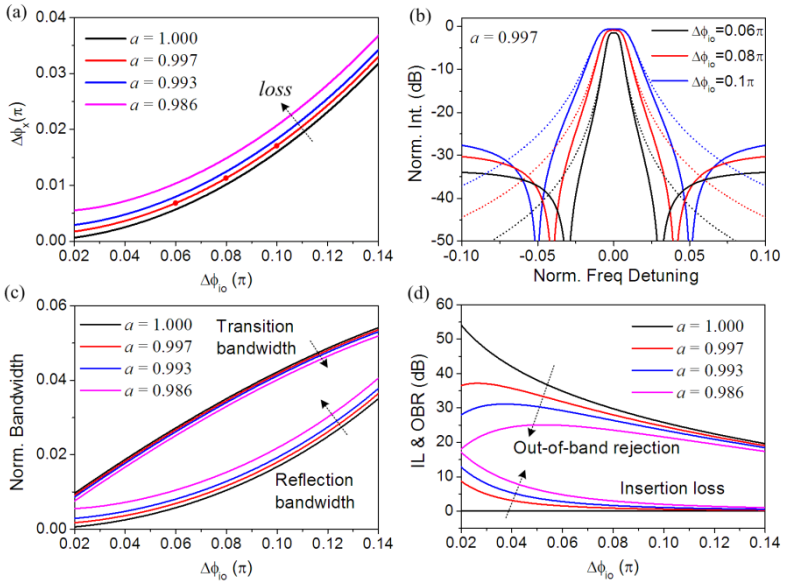

Fig. 3. (a) Relation between $\Delta\phi_x$ and $\Delta\phi_{io}$ for flap-top filters. (b) Solid curves: reflection intensity spectra of our device; dotted curves: drop-port intensity spectra of an add-drop filter. (c) FSR-normalized transition and reflection bandwidths as functions of $\Delta\phi_{io}$. (d) Insertion loss and out-of-band rejection ratio as functions of $\Delta\phi_{io}$. In (b)-(d), the flap-top passband condition is satisfied.

The reflection bandwidth is defined as the frequency separation between the poles. *i.e.*, $BW_{ref} = \tan^{-1}(\kappa_x/t_{io}t_x)/\pi$ (normalized to the free spectral range (FSR)). The roll-off rate is related to the transition bandwidth, defined as the frequency separation between the pole and the zero, *i.e.*, $BW_{tran} = [\cos^{-1}(t_{io}t_x)\text{-}\tan^{-1}(\kappa_x/t_{io}t_x)]/2\pi$ (normalized to the FSR). Figure 3(c) shows BW_{ref} and BW_{tran} change with $\Delta\phi_{io}$ for various loss factors. Larger $\Delta\phi_{io}$ leads to a wider reflection passband but a slower roll-off. Phase shift $\Delta\phi_{io}$ not only affects the filter bandwidth but also the insertion loss and out-of-band rejection ratio (or the cross-talk level). The normalized reflection intensity at the resonance frequency is $I_{r0} = |H_r(1)|^2$, and thus the insertion loss (at the reflection end) is $IL = -20\lg(|H_r(1)|)$. The out-of-band rejection ratio is defined as $OBR = 20\lg(|H_r(1)|/|H_r(-1)|)$, indicating the contrast between the on- and off-

#140999 - $15.00 USD Received 13 Jan 2011; revised 1 Apr 2011; accepted 1 Apr 2011; published 12 Apr 2011

resonance reflection intensities. Figure 3(d) shows the *IL* and *OBR* of the flat-top filter change with $\Delta\phi_{io}$ for various loss factors. Larger $\Delta\phi_{io}$ has lower insertion loss but higher cross-talk level.

The waveguide loss also plays an important role in the filter performances. Under the flat-top passband condition and with a certain $\Delta\phi_{io}$, larger waveguide loss slightly increases the reflection bandwidth but also deteriorates the filtering performance in terms of insertion loss and cross-talk level as seen from Figs. 3(c) and 3(d). For narrow-bandwidth filters ($\Delta\phi_{io}$ is small), loss can more significantly degrade its performances, because a narrow bandwidth means a high-Q resonance and hence it is more sensitive to loss.

4.3 Tunable delay line

As like microring resonators, group delay is greatly enhanced around resonance, making it suitable for optical signal delay applications. Neglecting the linear transmission factor t_{wg} in Eq. (7), the reflection group delay at the uncoupled resonance frequency (the operating frequency) can be expressed as

$$\tau_g\big|_{\phi=0} = 2T_R\left[\frac{1-r_0}{1+|p_0|^2-2r_0} - \frac{1-r_0}{1+|z_0|^2-2r_0}\right], \tag{17}$$

where $r_0 = \mathrm{Re}(z_0) = \mathrm{Re}(p_0) = at_{io}t_x$ is the real part of the zeros and poles. Note that $|p_0| < |z_0|$, and therefore, the group delay is always positive. Similarly, group delay can also be achieved from the transmission port. In the following analysis, we only focus on the reflection port, as it has a low insertion loss and can simultaneously perform channel dropping and delay functions.

As phase changes nonlinearly with frequency around resonance, GDD can be strong enough to significantly distort the optical signal. At the operating frequency, even dispersive orders of GDDs are all zero, but odd dispersive orders of GDDs still exist. To flatten the group delay, the third order GDD should be zero at the operation frequency, *i.e.*, $d^3\Phi_r(\phi)/d\phi^3 = 0$ at $\phi = 0$, where $\Phi_r(\phi)$ is the phase of $H_r(z)$. From Eq. (7) and after some mathematical manipulation, we get the condition for the flat-top group delay response:

$$\left|\frac{1-z_0}{1-p_0}\right|^6 = \frac{2r_0^2+\left(|z_0|^2+1\right)r_0-4|z_0|^2}{2r_0^2+\left(|p_0|^2+1\right)r_0-4|p_0|^2}\cdot\frac{1-|z_0|^2}{1-|p_0|^2}. \tag{18}$$

For the lossless case ($a = 1$), the above equation can be simplified to

$$2r_0^2+\left(|p_0|^2+1\right)r_0-4|p_0|^2 = 0. \tag{19}$$

Therefore, the pole and zero should satisfy Eq. (18) or Eq. (19) to achieve a flat-top group delay response. Substituting p_0 with Eq. (14), Eq. (19) becomes

$$\frac{1-t_x t_{io}}{\kappa_x} = \sqrt{\frac{4}{t_x t_{io}}-1} \approx \sqrt{3}. \tag{20}$$

In terms of $\Delta\phi_x$ and $\Delta\phi_{io}$, Eq. (20) can be rewritten as

$$\Delta\phi_x \approx \sqrt{3}-\sqrt{3-\Delta\phi_{io}^2}. \tag{21}$$

Hence, for low loss and high optical delay cases, $\Delta\phi_x$ and $\Delta\phi_{io}$ have a simple relation given by Eq. (21).

Figure 4(a) shows the dependence of $\Delta\phi_x$ on $\Delta\phi_{io}$ for different loss factors based on Eq. (18). $\Delta\phi_x$ is almost linearly proportional to $\Delta\phi_{io}$ in a small range of interest, which implies that $\Delta\phi_x$ and $\Delta\phi_{io}$ can be simultaneously tuned by one external voltage as long as their corresponding active region lengths are in scale. This can greatly simply the drive circuit for

#140999 - $15.00 USD Received 13 Jan 2011; revised 1 Apr 2011; accepted 1 Apr 2011; published 12 Apr 2011

group delay tuning. Figure 4(b) shows the insertion loss changes as a function of $\Delta\phi_{io}$. Higher waveguide loss increases the insertion loss, similar to the flat-top filter case. Yet distinct from the previous case, larger $\Delta\phi_{io}$ can also lead to a higher insertion loss, more evident for the lossless case (a = 1), as not all light is reflected back at the operating frequency. Figures 4(c) and 4(d) show the group delay bandwidth (approximately the filter bandwidth) and group delay (at the operating frequency) change as functions of $\Delta\phi_{io}$. A large group delay can be obtained by using smaller $\Delta\phi_{io}$ and $\Delta\phi_x$ yet with a sacrifice of smaller bandwidth, limited by the so-called delay-bandwidth product in resonance systems [32]. Large group delay corresponds to a high-Q resonance, which is more sensitive to loss. A small increase in loss can significantly deteriorate its group delay response. Hence, to get a high group delay, not only should $\Delta\phi_{io}$ and $\Delta\phi_x$ be small, the loss should also be kept low enough.

Figures 4(e) and 4(f) show the normalized reflection intensity and group delay spectra for $\Delta\phi_{io} = 0.06\pi$, 0.08π and 0.1π. As the third-order GDD is eliminated at the operating frequency, the group delay is almost flat within its bandwidth, and it can be continuously tuned for a relatively large range. For instance, if the device size is $L = L_1+L_2+L_3 = 60$ μm, the waveguide group refractive index $n_g = 4.0$, and the loss factor $a = 0.997$ (corresponding to a 5 dB/cm average waveguide propagation loss), then FSR ≈ 10 nm and $T_R \approx 0.8$ ps at 1.55 μm wavelength, and the group delay thus can be continuously tuned for 28 ps with its bandwidth kept >10 GHz.

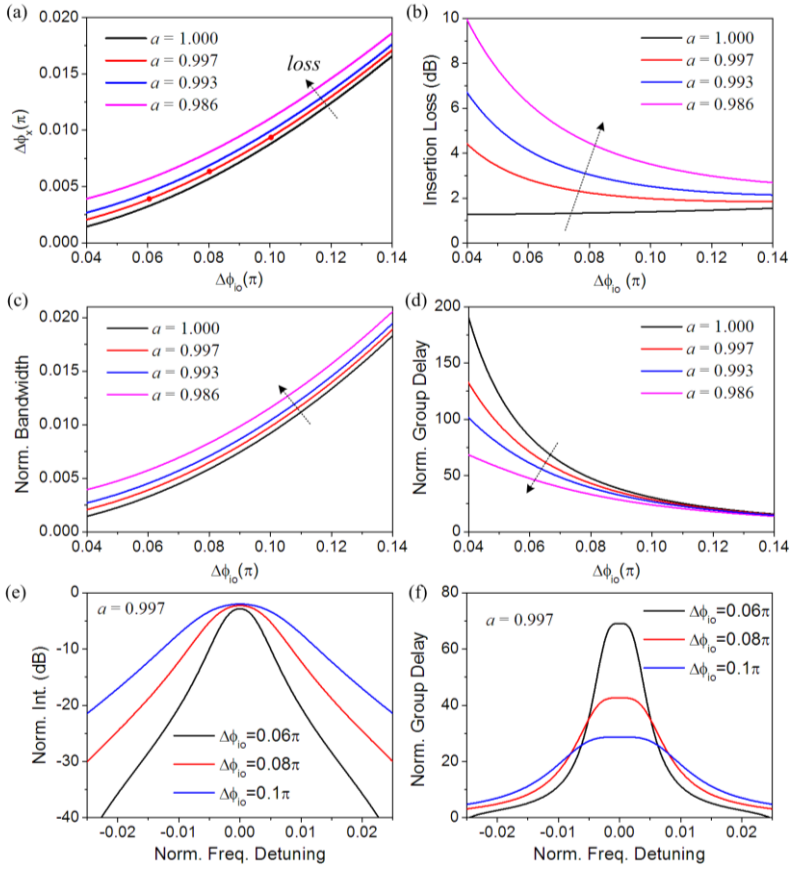

Fig. 4. (a) Relation between $\Delta\phi_x$ and $\Delta\phi_{io}$ for flap-top group delay responses. (b)-(d) Insertion loss, normalized group delay bandwidth, and group delay change as functions of $\Delta\phi_{io}$. (e) and (f) Typical reflection intensity and group delay spectra. In (b)-(f), the flat-top group delay condition is satisfied.

#140999 - $15.00 USD Received 13 Jan 2011; revised 1 Apr 2011; accepted 1 Apr 2011; published 12 Apr 2011

We also compare our device to a conventional double-ring ADF for signal delay application. In the ADF configuration, the resonances of the two rings should be well-aligned and the coupling strength of the three couplers (input, output and inter-ring couplers) should be well-controlled in order to obtain flat-top group delay responses. Yet in our structure, the resonances are always aligned because they are from degenerate CW and CCW modes of one physical resonator, and hence it alleviates the stringent fabrication requirement. Moreover, our structure has only two tuning elements compared to three in the double-ring ADF, so it is more compact and has less parameters to control, resulting in easy tuning and less power consumption.

Figure 5 shows the total phase shift as a function of group delay for our device and a double-ring ADF. The ADF-based tunable delay line structure is schematically illustrated in the inset. As the mutual mode coupling is much weaker than the input/output coupling (evident from Eq. (21)), the total phase shift for our device is nearly half of that for the ADF structure. The phase shift can be implemented by free carrier injection in silicon [31], and thus the power consumption is also almost one half less for our structure. Likewise, for resonance frequency tuning, because both CW and CCW modes can be simultaneously tuned by one waveguide section (*e.g.*, waveguide L_1) in our structure, the power consumption spent on the frequency tuning is also one half smaller for our structure.

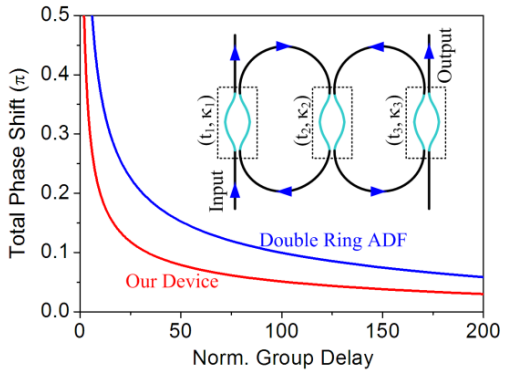

Fig. 5. Comparison between our device and a double ring ADF delay line in terms of total phase shift versus group delay.

4.4 Tolerance to structural parameters

In the previous analysis, we assume the input and output couplers are both ideal 3-dB couplers. However, in reality, due to fabrication errors, the waveguide width and gap separation between waveguides are hard to control very precisely, and as a result, the coupling strength always deviates from what is designed. To investigate how the performances of the high-order filter and delay line deteriorate from the optimum ones, we resort to Eqs. (1)-(5) to numerically calculate the reflection intensity and group delay spectra.

For the filter configuration, we fix the phase tuning parameters at $\Delta\phi_{io} = 0.08\pi$ and $\Delta\phi_x = 0.011\pi$ and vary the input and output coupling ratios. Figures 6(a)-6(c) show the reflection spectra for various combinations of t_a^2 and t_b^2. When the input and output coupling ratios are balanced, *i.e.*, $t_a^2 = t_b^2$, the filter spectrum is always symmetric, as shown in Fig. 6(a). The imperfection of the input and output couplers (non-ideal 3-dB couplers) causes the filter passband rounded and broadened. If only one of the couplers is imperfect, then the passband becomes slightly rounded and inclines towards one side, with its central wavelength shifts a little bit, as shown in Fig. 6(b). The most interesting combination is when the couplers are complementary, *i.e.*, $t_a^2 + t_b^2 = 1$. In this case, the passband top remains almost flat while it inclines towards one side, as shown in Fig. 6(c). From these plots, it can be seen that if the

#140999 - $15.00 USD Received 13 Jan 2011; revised 1 Apr 2011; accepted 1 Apr 2011; published 12 Apr 2011

variation of t_a^2 and t_b^2 is within ±0.1, the high-order filtering performance is still reasonably good.

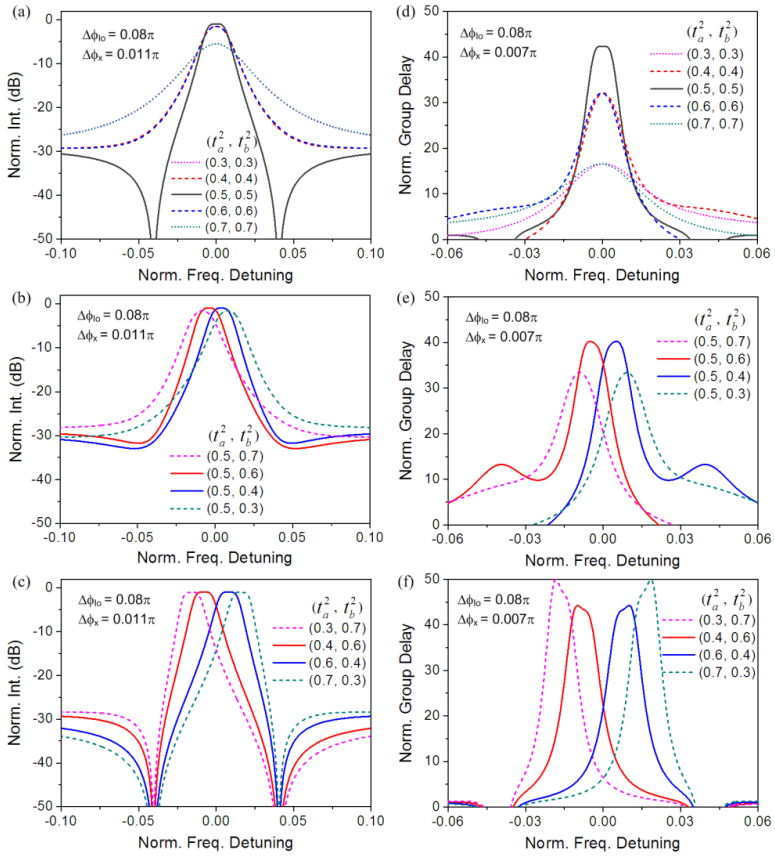

Fig. 6. (a)-(c) Reflection intensity spectra for various input and output coupling ratios. (d)-(f) Reflection group delay responses for various input and output coupling ratios.

For the delay line configuration, we fix the phase tuning parameters at $\Delta\phi_{io} = 0.08\pi$ and $\Delta\phi_x = 0.007\pi$. The imperfection of the couplers also degrades the delay line performance with a similar trend as in the filter case. For the complimentary combination of t_a^2 and t_b^2 (Fig. 6(f)), the larger the difference between t_a^2 and t_b^2 is, the sharper the group delay curve becomes. As the passband inclines to one side, the corresponding transition band becomes narrower (faster roll-off) and thus the phase change becomes more rapid, leading to a high group delay. It can be seen that the group delay is still within an acceptable level, if the coupling ratio change is within ±0.1.

Besides the input and output couplers, the MZI crossing coupler also plays a significant role in the device performances. The imperfection of the MZI coupler causes the mutual-mode coupling coefficient κ_x to only value in a limited range, or in other words, κ_x cannot be very small and thus the filter and delay line bandwidth cannot be very narrow. However, as long as Eqs. (16) and (18) are satisfied, the flat-top passband and group delay responses still can be obtained.

To reduce the coupling sensitive to fabrication errors, multimode interference (MMI)-based couplers can be used instead of directional couplers. MMI-based couplers are based on self-imaging to achieve the power splitting, and therefore, they are more resilient to the structural dimension change, although they suffer from a higher loss [33].

#140999 - $15.00 USD Received 13 Jan 2011; revised 1 Apr 2011; accepted 1 Apr 2011; published 12 Apr 2011

As like most resonance structures, our structure is also sensitive to the environment temperature fluctuation (if the waveguide is not specially designed). The influence of the temperature change can be modeled by varying n_{eff} and the coupling coefficients. Due to the symmetry of the structure, the interference paths (except the resonance loop back interference) are all balanced, and therefore, the change in n_{eff} causes the intensity and group delay spectra to only experience a shift without any change in their profiles. The coupling change has a more negative effect on the device performances as discussed previously. For a typical silicon wire waveguide-based 3-dB directional coupler, our simulation based on beam propagation method (BPM) shows that temperature increases by 10 °C, coupling ratio only changes by <1%, which has an almost negligible effect according to Fig. 6. To stabilize the device over temperature variation, athermal waveguide design can be employed [34].

5. Conclusion

In conclusion, we presented a novel reconfigurable resonance structure, formed by a single self-coupled waveguide, to function as a tunable filter and a tunable delay line. Due to the self-coupling of the waveguide, both the CW and CCW resonance modes are excited with their input/output and mutual mode coupling strengths controlled by two push-pull phase shifters. Using the transfer-matrix method, we got the z-domain transfer functions for the transmission and reflection ports, and their optical characteristics under different configurations were analyzed. In particular, we analyzed its optical performances as a tunable second-order filter and a low-dispersion delay line. The requirements for the two phase shifters to get the flat-top filtering and group delay responses were deduced, providing a guideline for the device design. As the coupled resonances are provided by the CW and CCW modes of one physical resonator, the need for accurate alignment of resonance frequencies is no longer necessary. Compared to conventional coupled microring resonators, our resonance structure is more compact and the power consumption for reconfiguration is lower, which is especially important for future large-scale integrated photonic chips.

Acknowledgement

This work was supported in part by the 973 Program (2011CB301700), the National Natural Science Foundation of China (NSFC) (61007039 and 61001074), the Science and Technology Commission of Shanghai Municipality (STCSM) Project (10DJ1400402, 09JC1408100), and the State Key Lab Projects (GKZD030020).

#140999 - $15.00 USD Received 13 Jan 2011; revised 1 Apr 2011; accepted 1 Apr 2011; published 12 Apr 2011